How Much Do Different Land Models Matter for Climate Simulation? Part I: Climatology and Variability

JIANGFENG WEI, PAUL A. DIRMEYER, ZHICHANG GUO, AND LI ZHANG

Center for Ocean–Land–Atmosphere Studies, Calverton, Maryland

VASUBANDHU MISRA

Department of Meteorology and Center for Ocean–Atmosphere Prediction Studies, The Florida State University, Tallahassee, Florida

(Manuscript received 2 April 2009, in final form 23 November 2009)

ABSTRACT

An atmospheric general circulation model (AGCM) is coupled to three different land surface schemes (LSSs), both individually and in combination (i.e., the LSSs receive the same AGCM forcing each time step and the averaged upward surface fluxes are passed back to the AGCM), to study the uncertainty of simulated climatologies and variabilities caused by different LSSs. This tiling of the LSSs is done to study the uncertainty of simulated mean climate and climate variability caused by variations between LSSs. The three LSSs produce significantly different surface fluxes over most of the land, no matter whether they are coupled individually or in combination. Although the three LSSs receive the same atmospheric forcing in the combined experiment, the inter-LSS spread of latent heat flux can be larger or smaller than the individually coupled experiment, depending mostly on the evaporation regime of the schemes in different regions. Differences in precipitation are the main reason for the different latent heat fluxes over semiarid regions, but for sensible heat flux, the atmospheric differences and LSS differences have comparable contributions. The influence of LSS uncertainties on the simulation of surface temperature is strongest in dry seasons, and its influence on daily maximum temperature is stronger than on minimum temperature. Land–atmosphere interaction can dampen the impact of LSS uncertainties on surface temperature in the tropics, but can strengthen their impact in middle to high latitudes. Variations in the persistence of surface heat fluxes exist among the LSSs, which, however, have little impact on the global pattern of precipitation persistence. The results provide guidance to future diagnosis of model uncertainties related to LSSs.

1. Introduction

One of the largest uncertainties in climate simulations is from the representation of land processes, because there are few observations to calibrate or constrain them. Different land surface schemes (LSSs) use quite different parameterizations to describe the complex hydrological, biogeophysical, and biogeochemical processes. To investigate the uncertainties in the behavior of LSSs and their influence on climate simulations, the Project for Intercomparison of Land Surface Parameterization Schemes (PILPS) was established (Henderson-Sellers et al. 1995, 1996; Pitman and Henderson-Sellers 1998; Pitman et al. 1999). PILPS compared offline simulation from over 20 LSSs at several different locations and found that, even when forced by the same atmospheric forcing and provided the same parameter settings, different LSSs can still give significantly different surface fluxes. When these LSSs are coupled to the atmospheric general circulation models (AGCMs), their different behaviors will bring uncertainties into the simulated climate. Realizing this, PILPS compared the simulation results from some of the LSSs as a component of the Atmospheric Model Intercomparison Project (AMIP; Gates 1992; Phillips 1994) GCMs (Qu and Henderson-Sellers 1998; Henderson-Sellers et al. 2003; Irannejad et al. 2003). However, as the LSSs are coupled to different AGCMs, this comparison was inconclusive.

More than a decade ago, there was a European project with the aim of determining the uncertainties linked to land surface processes in climate change simulations

Corresponding author address: Jiangfeng Wei, COLA/IGES, 4041 Powder Mill Road, Suite 302, Calverton, MD 20705.
E-mail: jianfeng@cola.iges.org

DOI: 10.1175/2010JCLI3177.1

(Polcher et al. 1998). Four GCMs, each coupled to two different LSSs, were used to explore the uncertainties in the simulation of present and future climate (Crossley et al. 2000; Gedney et al. 2000). Their main conclusion was that the choice of LSSs has a significant contribution to the simulated hydrological cycle and surface temperature, and its contribution to the simulation of climate change is even larger than that of the present climate. Most of the GCMs in this study were not coupled to completely independent LSSs, because they only altered some hydrological processes in the LSS. Likewise, Desborough et al. (2001) performed coupled model simulations with different land surface energy balance configurations of a single LSS. There are other similar comparison studies (e.g., Leplastrier et al. 2002; Pitman et al. 2004; Bagnoud et al. 2005) that have shown the sensitivity of climate simulation to the degree of LSS complexity.

Timbal and Henderson-Sellers (1998) examined the sensitivity of a regional weather forecast model to coupling to several LSSs. They found significant differences in surface fluxes and atmospheric response, but these integrations were very short and there was no chance for the atmosphere to equilibrate to the various land schemes. Xue et al. (2004, 2006) compared the simulations of monsoons with an AGCM coupled to two LSSs of different complexities, and found significant shifts in rainfall patterns. Cornwell and Harvey (2008) created a simple land scheme that mimics the behavior of many more complex schemes. They determined that for soil moisture, approximately half of the variability among the three atmosphere–ocean climate models was due to the different land schemes, and half came from different climatologies of the AGCMs. These studies are useful to investigate the role of different land surface parameterizations, but their results do not represent the general uncertainties among existing LSSs because of the subjectively specified changes or simplifications, short duration, and/or the small sample size.

Because the land–atmosphere system is nonlinear, uncertainties from LSSs can be amplified or reduced during land–atmosphere interaction. Qu and Henderson-Sellers (1998) compared the scatters from LSS offline simulations and those from AMIP simulations in which these LSSs are coupled to AGCMs. Their analysis at two locations shows that the range of scatter from the coupled AMIP simulations is larger than that from the offline simulations. However, Irannejad et al. (2003) developed pseudo-LSSs (PLSSs) by multivariable linear regressions of the AGCM outputs, and found that driving the PLSSs with the same atmospheric forcing at three river basins can increase the spread of annual latent heat (LH) flux compared to the coupled AGCM simulations. These contradictory conclusions may be caused by the AGCM differences in AMIP simulations or an insufficient number of study locations.

In this study, we show results from an AGCM coupled to three state-of-the-art LSSs. Instead of investigating the impact of a certain parameterization change, we try to investigate the composite uncertainties of the three LSSs and their influence on climate simulation. We also explore the influence of land–atmosphere coupling on the simulation uncertainties. Our focus will be on the global geographic variations of model uncertainties and land–atmosphere feedbacks, which generally have not been addressed in previous studies. In summary, the purpose of this study is threefold: first, to investigate current uncertainties in the behavior of LSSs; second, to investigate how much these uncertainties can influence atmospheric simulation through land–atmosphere interaction; and third and most importantly, to have a better understanding of the mechanisms of land–atmosphere coupling. All three purposes are addressed in this paper, while the companion paper (Wei et al. 2010, hereafter Part II) expands upon the third purpose.

2. Models and experiments

a. AGCM

The AGCM used is a recent version (version 3.2) of the Center for Ocean–Land–Atmosphere Studies (COLA) AGCM (Misra et al. 2007), which is based on the previous version (Kinter et al. 1997). It has 28 vertical sigma levels, and the horizontal resolution is T62 ($\sim 1.9° \times 1.9°$). The model uses the relaxed Arakawa–Schubert deep convection scheme (Moorthi and Suarez 1992), the nonlocal boundary layer vertical diffusion scheme (Hong and Pan 1996), the longwave radiation scheme of the National Center for Atmospheric Research (NCAR) Community Atmosphere Model, version 3 (CAM3; Collins et al. 2002), and the cloud radiation scheme of the NCAR Community Climate Model version 3 (CCM3; Kiehl et al. 1998).

b. LSSs

Three LSSs are coupled to the AGCM in this study: a new version of the Simplified Simple Biosphere Model (SSiB; based on Xue et al. 1991; Dirmeyer and Zeng 1999), the recently released Community Land Model (CLM), version 3.5 (Oleson et al. 2004, 2008), and a recent version of Noah land model (version 2.7; Ek et al. 2003). These models have been widely used in weather and climate research.

This version of SSiB has some improvements over the previous version, which participated in the Second Global

Soil Wetness Project (GSWP-2; Dirmeyer et al. 2006) and the Global Land–Atmosphere Coupling Experiment (GLACE; Koster et al. 2006). Principally, the number of soil layers in the root zone has increased to four, and a three-layer snow model (Stieglitz et al. 2001) has been coupled to SSiB to replace the original simple snow parameterization. The new version uses the same schemes as that of CLM (Oleson et al. 2004) to calculate soil thermal conductivity and soil temperature. Preliminary results show that the new version has corrected a dry bias over much of the globe when coupled with the COLA AGCM, and the snow cover is better simulated.

Version 3.5 of CLM also has many important improvements compared to the previous version (CLM version 3), which participated in GLACE. The modifications include a new surface dataset, new parameterizations for canopy integration and interception, frozen soil, soil water availability, and soil evaporation, a TOPMODEL-based scheme for surface and subsurface runoff (Niu et al. 2005), a groundwater model for determining water table depth (Niu et al. 2007), and the introduction of a factor to simulate nitrogen limitation on plant productivity. CLM3.5 exhibits significant improvements in its hydrological cycle, which result in wetter soils, less plant water stress, increased transpiration and photosynthesis, and an improved annual cycle of total water storage and runoff. See Oleson et al. (2008) for a detailed description of the improvements.

The Noah land model is an improved version of the Oregon State University (OSU) land model (Pan and Mahrt 1987) developed in the 1980s, but with significant changes (Koren et al. 1999; Ek et al. 2003). The model has four soil layers and the root zone depth is spatially varying (depending on vegetation classes) rather than fixed as in the OSU model. The cold season physics have been dramatically improved, including frozen soil physics and snowpack physics. There are also refinements to the formulation of soil evaporation, ground heat flux, canopy conductance, surface runoff and infiltration, and soil thermal conductivity. In comparison to the OSU model, the forecast skill of surface temperature and the simulation of some regional climatology and variability are significantly improved when Noah model is coupled to an AGCM (De Haan et al. 2007). This is an updated release of the Noah model that was used in GSWP-2, and its simulation skill of soil moisture was found to be among the best of the models (Guo and Dirmeyer 2006).

SSiB and Noah are ''second generation'' LSSs (e.g., Sellers et al. 1997), built around the explicit description of soil and vegetation processes involved in closure of the surface energy and water budgets. CLM is ''third generation,'' including the explicit representation of the role of carbon and nitrogen in modulating energy and water fluxes, although the carbon and nitrogen cycles are not enabled in our experiments. There are many specific differences among these LSSs in the parameterization and calculation of particular processes. In addition, the three LSSs have different numbers of soil layers and soil depths, and each uses its own soil and vegetation datasets. These different model boundary conditions cannot be easily changed to be the same because each LSS is developed with its own datasets of land cover and soil (Pitman et al. 2009). Therefore, the simulated differences among the LSSs are caused by differences in both model parameterizations and specified boundary conditions. The model integration and coupling are all conducted at a T62 spectral resolution with a common land–sea mask. The integration time step is the same for the LSSs and the AGCM (12 min). There is no tuning or nudging in the coupling for all of the models.

c. *Experiments and methods*

Two experiments are performed. In the first experiment (I), three LSSs are coupled to the AGCM individually and three separate integrations are performed. In the second experiment (C), an innovative coupling method is used to couple the three LSSs to the AGCM in combination (parallel) with a shared atmosphere. At each grid point and at every time step, the LSSs receive the same atmospheric forcing from the AGCM and the average surface fluxes from the LSSs are passed back to the AGCM. In fact, the same code is run for both experiment I and C integrations. The difference is effectively in the weights applied to the fluxes calculated by each LSS. Running with any single LSS is equivalent to assigning the fluxes from that scheme a weight of 1.0 and 0.0 for the other two. In experiment C, each LSS receives an identical $\frac{1}{3}$ weight, so each LSS has an equal opportunity to impact the atmosphere. This approach is analogous to that used in mosaic schemes (e.g., Koster and Suarez 1992), except that the tiles are complete LSSs and not just separate vegetation classes. From the perspective of the atmosphere, experiment C is simply a coupling to a fourth LSS with its own unique climatology and sensitivities. Depending on the degree of nonlinearities in the system, the equilibrium state that is reached should be different from the average of the three integrations in experiment I. The water and energy are conserved in experiment C (see the appendix).

The approach of experiment C is motivated by the success of ensemble multimodel approaches, such as the ''interactive ensemble'' for coupled ocean–atmosphere models (Kirtman and Shukla 2002) and multimodel ensembles for offline LSSs (Dirmeyer et al. 2006). Such multimodel approaches can give demonstrably better

simulations of key aspects of the climate system than individual models can attain. From the perspective of the land, experiment C is similar to running three land model offline experiments with the same atmospheric forcing, but here the atmosphere is affected by the average feedback from the LSSs. In this paper, we are comparing the behavior among the three LSSs in experiment C in the same way one would compare three offline integrations. We do this to understand the behavior of each scheme in this common modeling framework.

All of the simulations start from 1 April 1982 and end on 1 January 2005 (nearly 23 yr). The last 18 yr of data are used for analysis. The atmospheric initial condition is from National Centers for Environmental Prediction (NCEP)–NCAR reanalysis, and land initial conditions are from long-term offline runs forced by the 40-yr European Centre for Medium-Range Weather Forecasts (ECMWF) Re-Analysis (ERA-40; Uppala et al. 2005), except that the precipitation is corrected according to observations (Rudolf et al. 1994). Observed weekly sea surface temperature (Reynolds et al. 2002) is prescribed in all of the experiments.

3. Differences in model climatology

a. Surface energy and water fluxes

1) CLIMATOLOGY DIFFERENCES

Surface energy and water exchange is the key to understanding land–atmosphere interaction. We first look at the intermodel climatology differences of surface fluxes and their significances. Let us assume that $\overline{x}_1$ and $\overline{x}_2$ are the n-yr average of a variable from any two cases, and s_1^2 and s_2^2 are the interannual variances of the variable. Then, the test statistic,

$$t_{1,2} = \frac{|\overline{x}_1 - \overline{x}_2|}{\left(\frac{s_1^2}{n} + \frac{s_2^2}{n}\right)^{1/2}}, \tag{1}$$

follows the Student's t-test distribution with $n - 1$ degrees of freedom (Wilks 2006). In our case, $n = 18$, $\overline{x}_1$ and $\overline{x}_2$ are the 18-yr averages of the June–August (JJA) mean for two different models, and s_1^2 and s_2^2 are the interannual variances of the JJA mean. This test examines the significance of intermodel climatology differences relative to their interannual variability. At each grid point, we can calculate the average t for the three configurations as

$$\overline{t} = (t_{\mathrm{SSiB,CLM}} + t_{\mathrm{SSiB,Noah}} + t_{\mathrm{Noah,CLM}})/3. \tag{2}$$

Then, we can obtain the average confidence levels of their differences (left column of Fig. 1). Also shown, in the right column of Fig. 1, are their coefficients of variation (CV; i.e., the standard deviation divided by the mean) across the three models, which measure the intermodel climatology differences relative to their means. The following four variables, each from two experiments (except precipitation, which is identical for the three LSSs in experiment C), are shown: surface net radiation (Rnet), precipitation (P), sensible heat (SH) flux, and LH flux.

Generally speaking, LSS difference is the most important factor causing the simulated differences in land surface state and fluxes (e.g., Kato et al. 2007; Irannejad et al. 2003). Beyond that, precipitation and radiation are two most important forcings (e.g., Guo et al. 2006a; Wei et al. 2008b). LH and soil moisture are most strongly affected by precipitation, while SH is most strongly affected by radiation (Kato et al. 2007; Wei et al. 2009). It is useful to keep these points in mind when analyzing the results.

The left column of Fig. 1 shows that almost all of the land area has very significant intermodel differences for the variables. Precipitation difference is a little less significant over some high-latitude regions, probably because of the larger internal variability there. Although the differences are all significant, the percentage uncertainties (relative to their means) are quite different. The CVs for Rnet are small for both experiments, and most of the uncertainties are from net longwave radiation (not shown). For experiment C, Rnet uncertainties (caused by differences in albedo, emissivity, and surface temperature) can be regarded as the only uncertainty in forcing to the LSSs because downward fluxes are the same. The CVs of surface heat fluxes (SH and LH fluxes) are much larger than those of Rnet, with most of the land area exceeding 20%. This happens for both experiment I (different precipitation for LSSs) and experiment C (same precipitation), indicating that a large divergence in surface heat fluxes can be caused by the different surface energy partitions of the LSSs, even when precipitation is the same. Similar results are found in offline land model simulations (e.g., Liang et al. 1998; Pitman et al. 1999; Dirmeyer et al. 2006).

The patterns of CV for SH(I) and SH(C) are very similar, with SH(I) having larger amplitudes than SH(C). This indicates that the LSS differences largely determine the pattern of SH uncertainties, while these uncertainties can be amplified by radiation, precipitation, and other differences caused by land–atmosphere feedback. On the other hand, the patterns of CV for LH(I) and LH(C) are different, with the pattern of LH(I) very similar to that of P(I), suggesting the dominant influence of precipitation. We also examined the intermodel CVs of SH and LH for more than a dozen GSWP-2 models. Their patterns (not shown) are similar to that of SH(C) and LH(C) in Fig. 1,

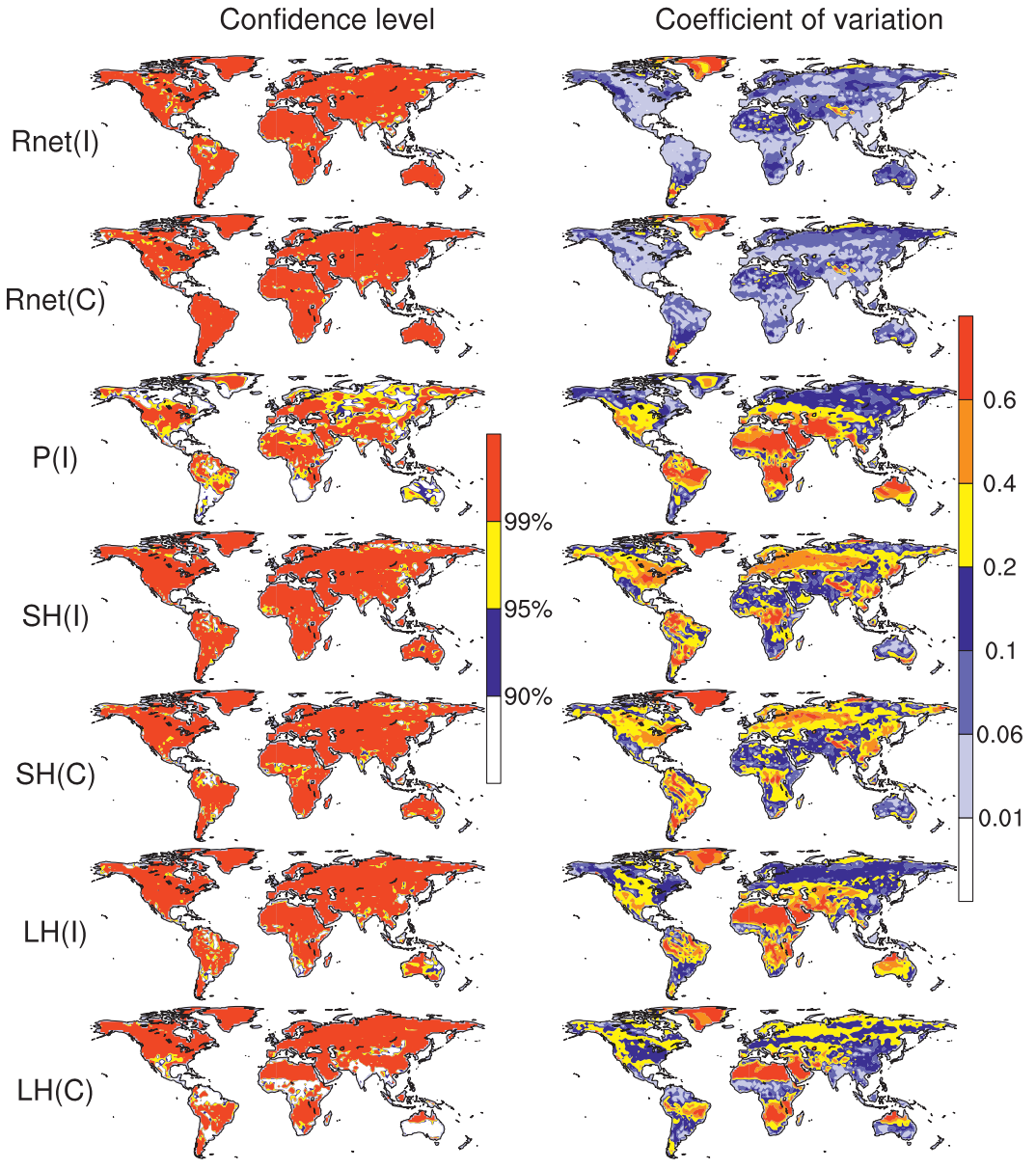

FIG. 1. (left) The mean confidence level of the JJA intermodel climatology differences among the three coupled models (see text for detailed description). (right) The intermodel coefficient of variation of the JJA climatologies across the three models. Each row is for a variable: Rnet, *P*, SH, and LH. Hereafter, the "I" and "C" in the brackets mean from experiments I and C, respectively.

implying that the three LSSs represent the uncertainties among many current LSSs fairly well.

2) EXPERIMENT I VERSUS EXPERIMENT C

Let Var(I) and Var(C) be the inter-LSS variances of average fluxes from land to atmosphere in experiments I and C, respectively. That is the variance across three different model climatologies. Intuitively, one might expect Var(I) to be larger than Var(C) because the LSSs receive the same atmospheric forcing in experiment C but not in I. This is generally true in Fig. 1. Thus, Var(I) is the intermodel variance that is caused by LSS differences and land–atmosphere feedback, while Var(C) is the variance caused by LSS differences only. Their difference Var(I) − Var(C) represents the variance caused by land–atmosphere feedback. Then, the ratio

$$\Phi = \frac{\mathrm{Var(I)} - \mathrm{Var(C)}}{\mathrm{Var(I)}} \tag{3}$$

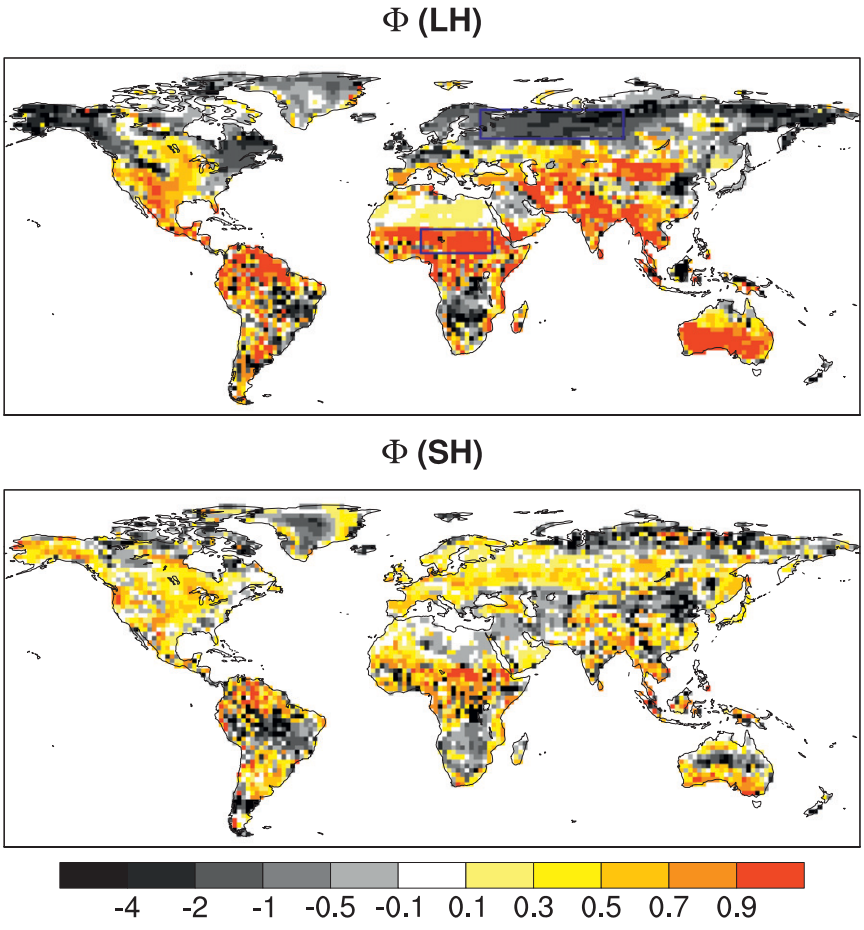

FIG. 2. The ratio Φ [see Eq. (3)] for the 1987–2004 average JJA (top) LH and (bottom) SH fluxes. The regions enclosed by blue boxes are for further analysis in Fig. 3.

represents the percentage of intermodel variance caused by land–atmosphere feedback, and $1 - \Phi$ represents the percentage of variance caused by LSS differences. If $\mathrm{Var(I)} \geq \mathrm{Var(C)}, 0 \leq \Phi \leq 1$. However, if $\mathrm{Var(I)} < \mathrm{Var(C)}$ ($\Phi < 0$), a negative feedback between land and atmosphere is implied and we cannot estimate the relative contributions of LSS differences and land–atmosphere interactions to the variance.

Figure 2 shows Φ averaged over JJA for SH and LH. Over most land areas, $0 \leq \Phi \leq 1$. However, there are still some areas with $\Phi < 0$. SH should have the same intermodel variance as LH if Rnet and the relatively small ground heat flux are the same for the LSSs. However, Rnet differs considerably among the models over some high-latitude and dry regions [Rnet(I) and Rnet(C) in Fig. 1]. This is why the Φ values of SH and LH differ most over these regions (Fig. 2).

To investigate the cause of the different spread changes (positive and negative Φ), we selected northern Eurasia and Sahel as two regions with strongly contrasting values of Φ (blue boxes in Fig. 2). Figure 3 shows the time series of LH, net shortwave radiation at surface (SWnet), total cloud cover, and precipitation over these two regions. It is evident that, compared to experiment I, the LHs in experiment C strongly converge in Sahel but diverge in northern Eurasia, consistent with the value of Φ. In the Sahel, the interannual time series of LH are negatively correlated with those of SWnet, but are positively correlated with those of cloud cover and precipitation. This is a semiarid, moisture-limited area, where evapotranspiration (ET) is nominally below the potential rate, so LH is strongly controlled by the land surface states, especially soil wetness, which is largely determined by rainfall. In experiment C, each LSS experiences the same rainfall, which leads to similar soil wetness and LH. In northern Eurasia, however, the correlation between SWnet and LH is positive for most of the time series. The soil moisture is plentiful in this region and the control on LH is mainly the availability of radiation at surface. The most significant change of LH is for CLM, when the LH

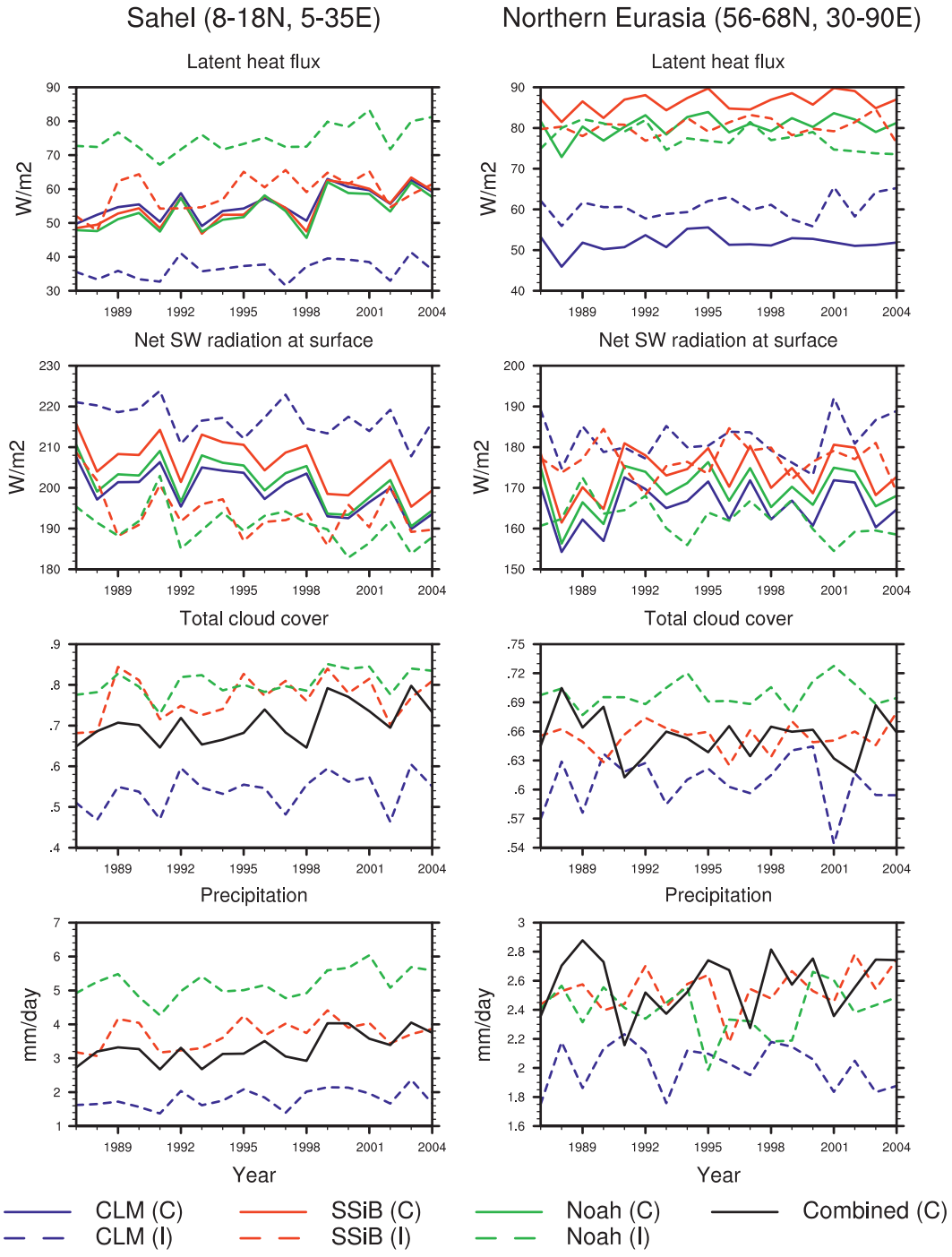

FIG. 3. The simulated 1987–2004 JJA average LH, SWnet, total cloud cover, and *P* for (left) the Sahel and (right) northern Eurasia. The areas of the two regions are marked by blue boxes in Fig. 2.

decreases greatly in experiment C compared to experiment I. The reason for the reduction is the decrease of net radiation at the surface caused by increased cloud cover. The soil is actually wetter, but this does not play a dominant role. The same mechanism applies to the Noah model. For SSiB, the condition is a little different. The small increase of LH in experiment C is accompanied by a small decrease of SWnet and a slight increase in precipitation. This indicates that different LSSs can have various thresholds between atmosphere control and soil moisture control over evaporation, even when under the same forcing. This increases the complexity of the problem.

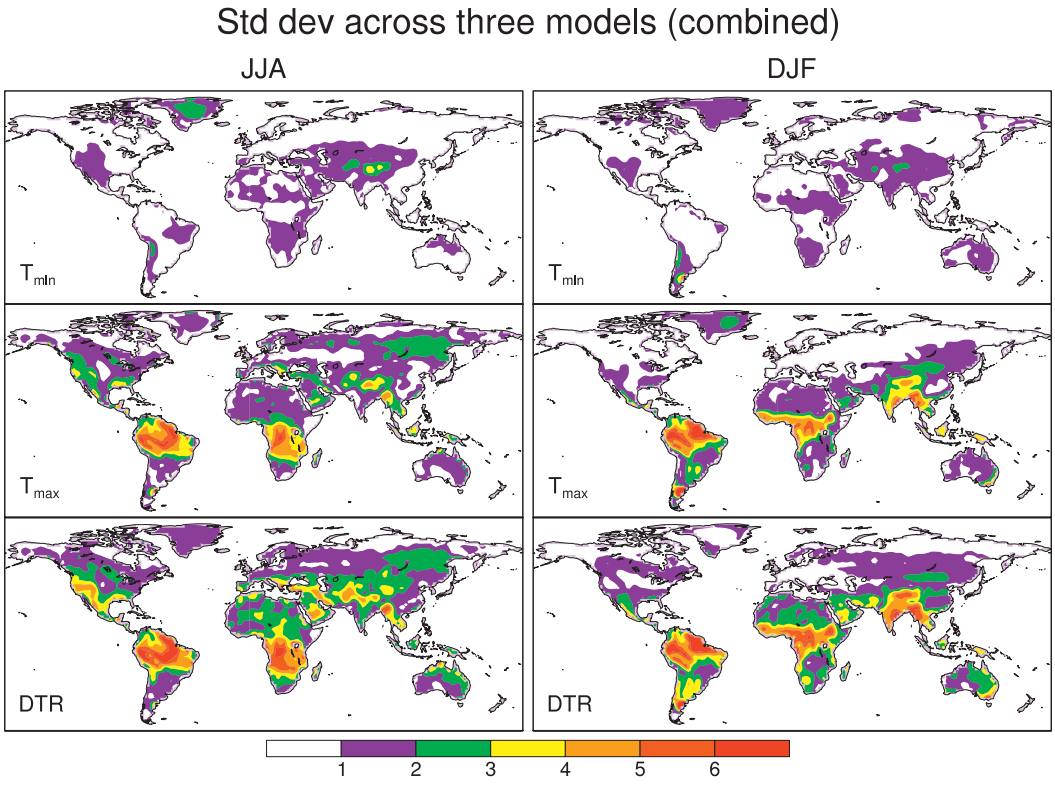

FIG. 4. The standard deviations of T_{min}, T_{max}, and DTR climatologies across the three LSSs in experiment C for (left) JJA and (right) DJF.

To summarize, in most regions the evaporation regime determines how the spread of LH among the LSSs changes. In regions where soil wetness is important for LH, such as arid and semiarid regions, the spread of LH can be larger when individually coupled, mostly caused by the different precipitation over land. In regions where soil is wet enough that ET is not stressed, the spread of LH decreases when individually coupled, which is mostly caused by the radiation changes associated with cloud cover changes.

The above mechanism can explain most of the distribution of Φ(LH) in Fig. 2. However, this mechanism cannot explain the negative values of Φ(LH) over southern Amazon, southern Africa, and northern Australia, which are all dry regions in the Southern Hemisphere. Given the same atmospheric forcing in experiment C, the LSSs have large divergences in LH relative to their mean [LH(C) in Fig. 1], indicating the large differences in the behavior of the LSSs over these regions. Coupling them to the AGCM individually can actually decrease the divergence. This is probably due to a negative feedback in experiment I: higher LH → lower surface temperature → lower precipitation → lower LH. This feedback does not happen over North Africa, where the precipitation amount is similarly low, because of the much higher temperatures. Therefore, the large difference in LSS behavior combined with a negative ET–precipitation feedback could be the reason for the negative values of Φ(LH) over these regions. On the other hand, the model bias in precipitation can influence the value of Φ(LH), for example, South Asia is too dry in the models, which may lead to unrealistic high values of Φ(LH).

For the colored area ($\Phi > 0$) in Fig. 2, Φ(LH) has much larger values than Φ(SH). This is because LH is more strongly influenced by precipitation, and the LSSs receive different precipitation in experiment I but the same precipitation in C. The largest values of Φ(LH) are generally over semiarid regions, where precipitation uncertainties strongly influence LH. Therefore, in experiment I, most of the intermodel difference of LH over semiarid areas is caused by the different precipitation over land. The uncertainties caused by LSS differences are generally small in these regions [LH(C) in Fig. 1]. For SH, only approximately half of the intermodel divergence is caused by the different forcings over land and the other half is from LSS differences. The similarity of the patterns between Φ(LH) and P(I) (Fig. 1)

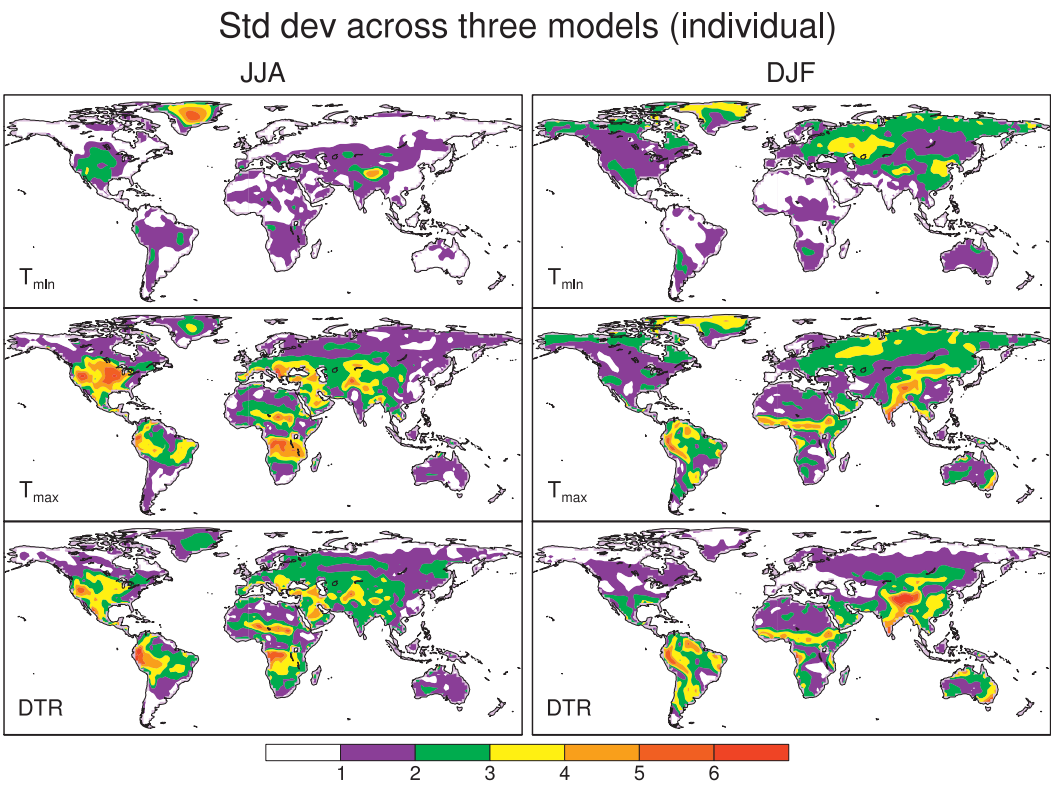

FIG. 5. Same as Fig. 4, but for experiment I.

and between Φ(SH) and SH(C) (Fig. 1) support this conclusion.

b. *Extreme temperature and its diurnal range*

Maximum and minimum surface temperatures (T_{min} and T_{max}) and diurnal temperature range (DTR = $T_{max} - T_{min}$) are important indicators of climate change. Observational data show that clouds and associated precipitation and soil moisture variations are the main cause for the variation of DTR over land (Karl et al. 1993; Dai et al. 1999). The increased cloud cover can sharply dampen the downward solar radiation during daytime and decrease T_{max}, and the associated precipitation and wet soil can strongly decrease T_{max} by promoting evapotranspiration. Both effects act to decrease the DTR. Other associated effects, like increased atmospheric water vapor, can increase both nighttime and daytime temperature and has little consequence for DTR. Within these feedback processes, the role of land processes is enclosed but is difficult to separate by analyzing observational data. Model experiments can separate the action processes and also provide more data for analysis. For example, Zhou et al. (2007, 2008) demonstrated by GCM experiments that vegetation removal and associated soil aridation can increase T_{min} much faster than T_{max} and also decrease DTR. Of course, model uncertainties exist.

Figure 4 shows the standard deviations of T_{max}, T_{min}, and DTR across the three LSSs in experiment C. Because different LSSs have different definitions and calculation methods for surface temperature, we compare the radiative temperature (skin temperature) of the LSSs. The latter should be very similar to surface temperature in amplitude and variability. Because the atmospheric forcing is the same, the standard deviation across the three LSSs is an indicator of the LSS uncertainties. Thus, Fig. 4 actually shows the influence of the LSS uncertainties on T_{max}, T_{min}, and DTR. It can be seen that the influence on T_{max} is much larger than on T_{min}, and most of the uncertainties in DTR are from T_{max}. The standard deviations evolve seasonally over most monsoon regions, with higher values during dry seasons. This is largely consistent with the evolution of LH uncertainties over these regions [LH(C) in Fig. 1, other seasons are not shown], indicating the importance of LH uncertainties on surface temperature and DTR over these regions. The large uncertainties over the northern Amazon basin seem to be related to the SH uncertainties [SH(C) in Fig. 1].

Figure 5 shows the standard deviations from experiment I. It differs from Fig. 4 in that each LSS now interacts with the atmosphere individually. By comparing the two figures, we can see the effect of land–atmosphere coupling

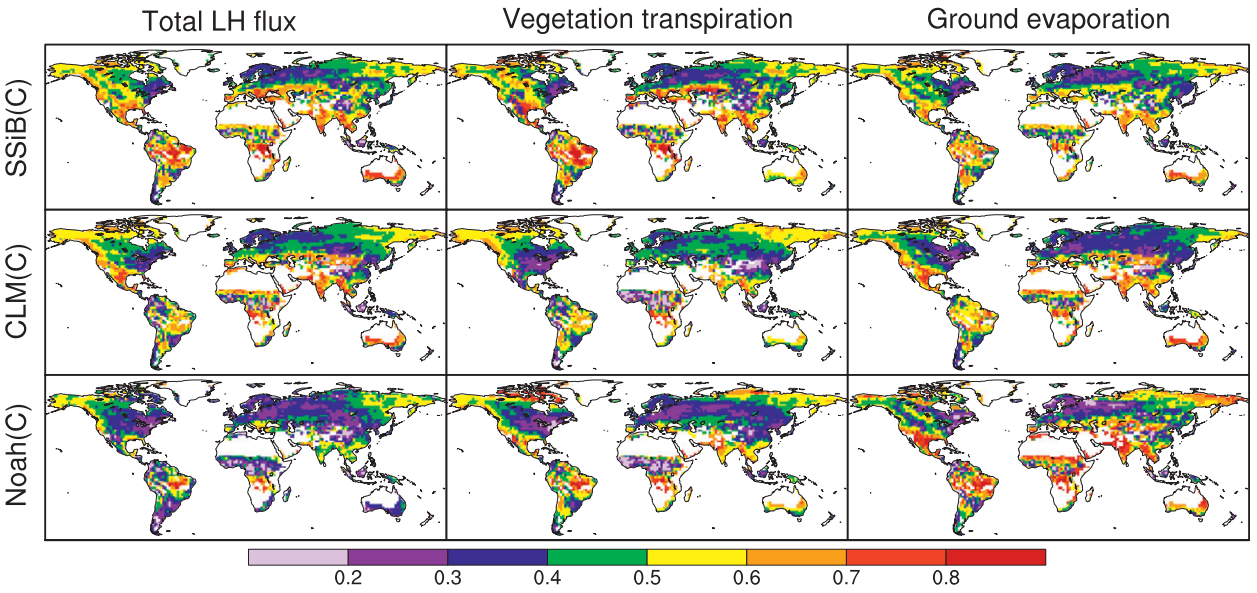

FIG. 6. The JJA lag-1-day autocorrelations of (left) total LH flux, (middle) vegetation transpiration, and (right) ground evaporation anomalies. The autocorrelations are calculated for each JJA and then averaged across 1987–2004. Seasonal cycles are removed before calculating the autocorrelations. Data from experiment C; experiment I shows similar results. (top) SSiB, (middle) CLM, and (bottom) Noah. The white areas over land are masked out using the same criteria as in Fig. 7. All the shaded areas are over the 95% confidence level.

on the uncertainties in surface temperature and DTR simulations. Compared to Fig. 4, Fig. 5 shows smaller uncertainties in the tropics, but larger uncertainties from the middle to high latitudes. The pattern of the JJA uncertainties in Fig. 5 is very similar to that of precipitation in Fig. 1, which suggests the dominant role of precipitation and cloud uncertainties. The decreased temperature uncertainties in the tropics could be related to a negative feedback there in experiment I: higher surface temperature → stronger convection → more precipitation and cloud → more ET and less radiation → lower surface temperature (Cook 1994; Zeng and Neelin 1999). This feedback affects T_{max} more than T_{min}. The increased temperature uncertainties in JJA over middle latitudes may be realized by a typical positive feedback: less precipitation and cloud → drier soil → less ET → higher surface temperature and less precipitation. In December–February (DJF), the increase of the uncertainties in T_{min} and T_{max} over high latitudes should be mainly from the complex snow–atmosphere–cloud feedback (Cess et al. 1991, 1996; Yang et al. 2001), which has large uncertainties among the models. However, this feedback seems to have weaker effect on DTR uncertainties, implying that it has a similar effect on both T_{min} and T_{max}.

In summary, the uncertainties of LH among the LSS strongly influence surface temperature, especially T_{max}. The influence is stronger in dry regions/seasons when LH has larger uncertainties. This influence of LSS uncertainties can be weakened in the tropics through a negative feedback, but can be strengthened in middle to high latitudes through a positive feedback (if warm) or the snow–atmosphere–cloud feedback (if cold).

4. Differences in model variability

a. Memory of land surface fluxes

Land surface influences climate variability mainly through its relatively long memory. The soil and vegetation can preserve the signal of past anomalous precipitation and temperature and exert their influence on current atmosphere (e.g., Koster and Suarez 1996, 2001; Wei et al. 2006; Hu and Feng 2004). Of all the different state and flux variables of land, LH may be the most important, because it directly connects to both the water and energy balance. Figure 6 shows the JJA lag-1-day autocorrelation of LH and its two components: vegetation transpiration and ground evaporation. Another component, canopy interception, generally has a memory less than a day and is not shown. We use data from experiment C to eliminate the possibility that the different memories are caused by different atmospheric forcing, so the memories of the LSSs can be compared.

It can be seen in Fig. 6 that, for the total LH, SSiB generally has the longest memory while Noah has the shortest memory. This is also true for vegetation transpiration. For ground evaporation, the memory of Noah is much higher than the other two. To better understand the reason for these differences, we look at the percentages of each component in total LH (Fig. 7). It is evident that, compared to the other two models, Noah has much

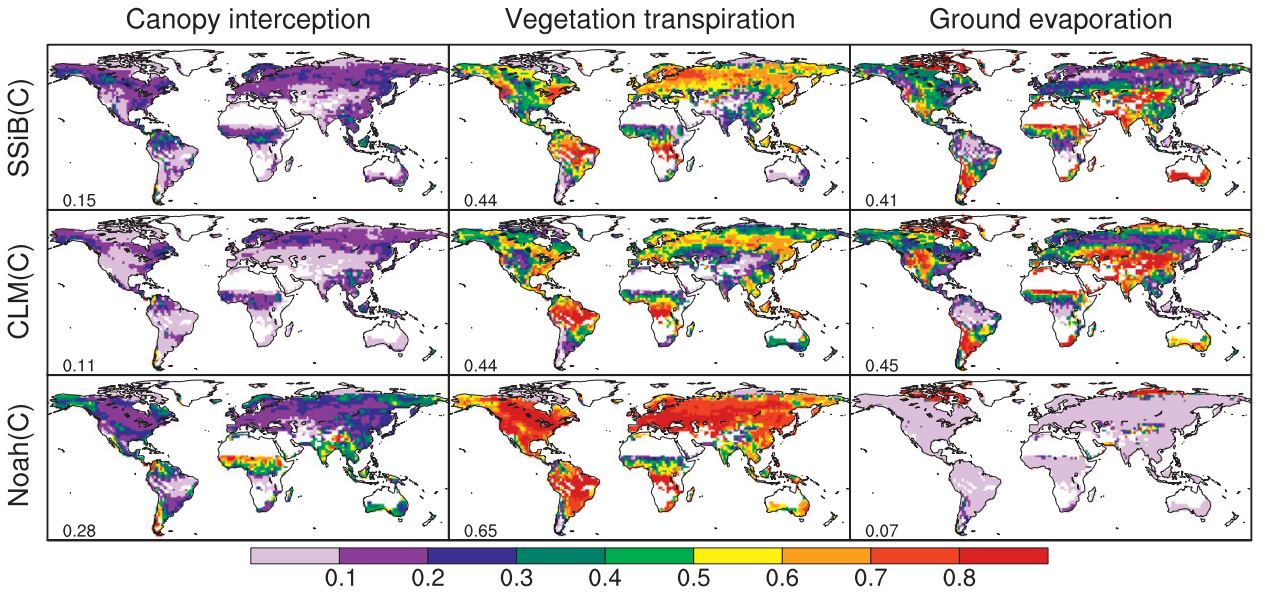

FIG. 7. The mean percentages of the three components in total LH flux during JJA (1987–2004): (left) canopy interception, (middle) vegetation transpiration, and (right) ground evaporation. Areas where the average total LH is less than 5 W m^{-2} or any flux component is negative for any of the models are not shaded for all the models. Data from experiment C; experiment I shows similar results. The global mean value of each panel is shown in the left corner.

larger percentages of LH from interception and transpiration, but a very small percentage from ground evaporation. Therefore, the source of the low memory of LH in Noah is interception and transpiration. Interception is a fast process while transpiration is a slow process. The low memory of LH for Noah in middle to high latitudes should be caused by the combined effect of relatively high percentage of interception and the relatively low memory of transpiration. Over the tropics, the low memory of Noah should be caused mainly by the high percentage of interception, because its memory of transpiration is similar to the other two models. The memory of SH for Noah is also lower than the other two models (not shown); SH and LH are connected in the surface energy balance equation and usually compensate each other.

b. *Precipitation persistence*

The memories inherent in the surface heat fluxes differ greatly among the LSSs. It would be interesting to examine how the different memories of land surface fluxes can influence precipitation variability. Figure 8 shows the lag-2-pentad precipitation autocorrelation in JJA. This method has been used in previous studies and is based on the assumption that a wetter soil caused by a storm may last several days and promote future storms (Koster et al. 2003). However, there is also a possibility that this persistence of precipitation is caused by the internal atmospheric dynamics or some other remote forcing (e.g., SST) and has nothing to do with soil moisture memory (Wei et al. 2008a). Note that the lag-2-pentad here and lag-1-day above have no specific physical meaning. They are just measures of memory based on the assumption that these processes are red noise processes. Increasing (decreasing) the time lag will decrease (increase) the value of autocorrelation, but the patterns change very little.

It can be seen in Fig. 8 that all of the model simulations show a largely similar pattern of precipitation persistence, but regional differences between models exist. The result from the combined simulation is within the range of the three individually coupled simulations. The average of the three individual simulations shows precipitation persistence that is larger than any of the individual simulations because the averaging tends to suppress the short-time-scale precipitation variations that are inconsistent between the models. Although the memory of surface LH and SH is much lower in Noah, it does not show an overall lower precipitation persistence than the other two models in the individually coupled simulations. This suggests that the land surface heat fluxes do not play a dominant role in the global pattern of precipitation temporal variability, but regional impacts may still exist. Compared to the observations, all simulations here have overestimated the precipitation persistence in many areas.

In Part II, we examine the connection of this precipitation persistence with precipitation predictability and land–atmosphere coupling.

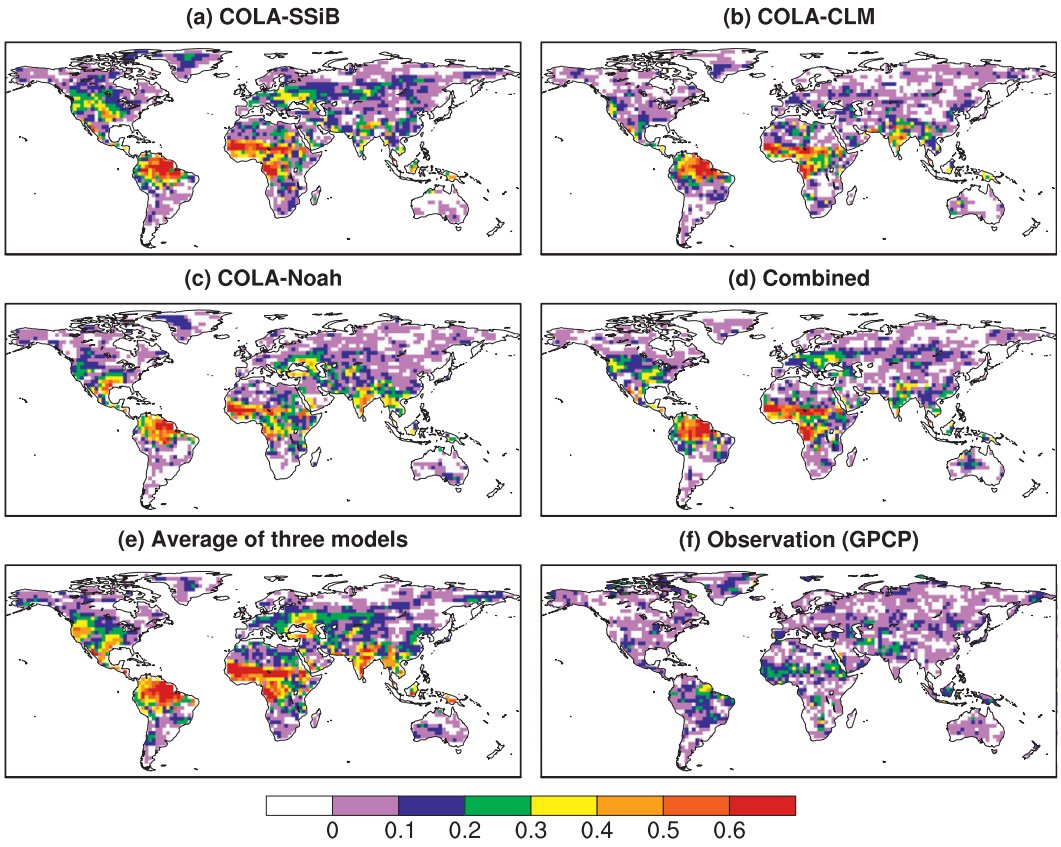

FIG. 8. The JJA lag-2-pentad autocorrelation of P across 1987–2004. (a) COLA–SSiB, (b) COLA–CLM, (c) COLA–Noah, (d) combined experiment, (e) calculated with the average precipitation of the three individually coupled simulations, and (f) from the observational dataset of GPCP (Xie et al. 2003). The model results are interpolated to the same grid as that of GPCP data (2.5° × 2.5°). Values larger than 0.11 are over the 95% confidence level. Seasonal cycles are not removed in this calculation; removing them can lead to results with similar patterns but smaller amplitude.

5. Conclusions and discussion

Three LSSs are coupled to an AGCM individually and in combination to study the uncertainties related to LSSs in climate simulation. This innovative coupling and comparison method has shown great potential for study of land–atmosphere interaction. By comparing the intermodel climatology and variability differences from a set of long-term AMIP-type experiments, we obtain the following conclusions:

1) There is a marked impact of the choice of LSS on the model hydrological cycle. The three LSSs give significantly different surface fluxes no matter whether in experiment I (different atmospheric fluxes to LSSs) or in experiment C (identical atmospheric fluxes to LSSs).
2) The evaporation regime (soil moisture limiting or radiation limiting) largely determines how the spread of LH among LSSs may change when they are coupled to an AGCM individually. Where soil moisture availability limits evapotranspiration, coupling the LSSs individually to an AGCM tends to increase the variance of LH among the models compared to offline simulations with the same atmospheric forcing. However, in areas where radiation availability determines LH, these fluxes can converge when LSSs are individually coupled.
3) In the individually coupled simulations, most of the LH uncertainties over semiarid areas are caused by the precipitation difference and LSS differences have very little influence. Meanwhile, only approximately half of the intermodel differences of SH over land are caused by the forcing difference and the other half is from LSS differences.
4) The uncertainties of LH among the LSSs have a strong influence on surface temperature, and it has more influence on T_{max} than on T_{min}. The influence is stronger in dry regions/seasons, where LH has more uncertainty. Land–atmosphere interaction can weaken the influence of LSS uncertainties in the tropics through a negative feedback, but may strengthen their influence

in middle to high latitudes through a positive feedback (in warm seasons) or the snow–atmosphere–cloud feedback (in cold seasons).

5) The memory of LH differs much among the LSSs. The memory of the Noah model is much lower than the other two, which is caused by a higher percentage of canopy interception in total LH and a shorter memory of vegetation transpiration. However, the global patterns of precipitation persistence are little influenced by this, although regional differences exist. Other external forcings, such as SST and radiation, play a more important role in this global pattern. All of the model simulations overestimate the precipitation persistence, which may impact the accuracy of the simulated land–atmosphere coupling. This is discussed further in Part II.

Our results provide guidance to future diagnosis of model uncertainties related to LSSs. The three LSSs may be considered to be a small but typical sample of our ability to simulate the system. Our results could be more representative with a larger sample size, but we believe the same qualitative results can be obtained with these three models. Indeed, these three LSSs show similar uncertainty patterns to those among GSWP-2 models. Note that we discuss the influence of LSS uncertainties on climate in this paper, which may be somewhat different from the general influence of land processes on climate. The impact discussed here is only related to uncertainties among LSSs, and the LSSs may have high consistency in some aspects, whose impact is not highlighted here.

The results obtained here may be affected by the forcing to LSSs. We use the method of combined coupling in experiment C, in which the forcing to the LSSs may not always be in the range of the three individually coupled runs in experiment I. Forcing the LSSs with the average fluxes and atmospheric conditions from experiment I may give a slightly different result. However, we believe the large-scale patterns and the mechanisms related to the interaction processes should be robust for different forcings.

We only investigate the uncertainties related to LSSs. It is likely that these results depend somewhat on the AGCM we used, and the way its PBL and convection parameterizations respond to variations in surface fluxes (Guo et al. 2006b). In fact, coupling of these three LSSs to other AGCMs is underway. By comparing a diverse sample of coupling configurations we would be able to better understand the potential interacting processes and uncertainties, a necessary step to improve the model simulation of land–atmosphere interaction.

Acknowledgments. This research was supported by National Oceanic and Atmospheric Administration Award NA06OAR4310067. Comments from three reviewers have enhanced the quality of the paper. The computing was completed on NCAR supercomputers. We thank NCEP EMC for providing the Noah land model. GPCP precipitation data were provided by the NOAA/OAR/ESRL PSD, Boulder, Colorado (available online at http://www.cdc.noaa.gov).

APPENDIX

Water Balance in Experiment C

On a global and annual average basis, the land surface water balance equation is

$$P = E + \Delta S + R, \tag{A1}$$

where P is precipitation, E is evapotranspiration, ΔS is soil moisture change, and R is runoff to the ocean. In experiment C, the precipitation to each LSS is identical, so their water balance equations are

$$P = E_{\mathrm{SSiB}} + \Delta S_{\mathrm{SSiB}} + R_{\mathrm{SSiB}}, \tag{A2}$$

$$P = E_{\mathrm{CLM}} + \Delta S_{\mathrm{CLM}} + R_{\mathrm{CLM}}, \quad \text{and} \tag{A3}$$

$$P = E_{\mathrm{Noah}} + \Delta S_{\mathrm{Noah}} + R_{\mathrm{Noah}}. \tag{A4}$$

Because the characteristics of the LSSs are different, E from one LSS may be much larger or smaller than that from another LSS, which may lead to differences in soil water storage and runoff between LSSs. Multiplying $\frac{1}{3}$ to each side of the Eqs. (A2)–(A4) and summing them, we get

$$P = (E_{\mathrm{SSiB}} + E_{\mathrm{CLM}} + E_{\mathrm{Noah}})/3 + (\Delta S_{\mathrm{SSiB}} + \Delta S_{\mathrm{CLM}} + \Delta S_{\mathrm{Noah}})/3 + (R_{\mathrm{SSiB}} + R_{\mathrm{CLM}} + R_{\mathrm{Noah}})/3. \tag{A5}$$

This is the water balance equation for the whole system. It is easy to find that no matter what weight is given to each LSS, as long as the sum of the weights is 1 and does not change over time, the water is conserved in the system. The energy balance in experiment C follows the same principle and is not shown here.

REFERENCES

Bagnoud, N., A. J. Pitman, B. McAvaney, and N. J. Holbrook, 2005: The contribution of the land surface energy balance complexity to differences in means, variances and extremes using the AMIP-II methodology. *Climate Dyn.,* **25,** 171–188, doi:10.1007/s00382-005-0004-9.

Cess, R. D., and Coauthors, 1991: Interpretation of snow-climate feedback as produced by 17 general circulation models. *Science,* **253,** 888–892.

——, and Coauthors, 1996: Cloud feedback in atmospheric general circulation models: An update. *J. Geophys. Res.,* **101** (D8), 12 791–12 794.

Collins, W. D., J. K. Hackney, and D. P. Edwards, 2002: An updated parameterization for infrared emission and absorption by water vapor in the National Center for Atmospheric Research Community Atmosphere Model. *J. Geophys. Res.,* **107,** 4664, doi:10.1029/2001JD001365.

Cook, K. H., 1994: Mechanisms by which surface drying perturbs tropical precipitation fields. *J. Climate,* **7,** 400–413.

Cornwell, A. R., and L. D. D. Harvey, 2008: Simulating AOGCM soil moisture using an off-line Thornthwaite potential evapotranspiration–based land surface scheme. Part I: Control runs. *J. Climate,* **21,** 3097–3117.

Crossley, J. F., J. Polcher, P. M. Cox, N. Gedney, and S. Planton, 2000: Uncertainties linked to land surface processes in climate change simulations. *Climate Dyn.,* **16,** 949–961.

Dai, A., K. E. Trenberth, and T. R. Karl, 1999: Effects of clouds, soil moisture, precipitation, and water vapor on diurnal temperature range. *J. Climate,* **12,** 2451–2473.

De Haan, L. L., M. Kanamitsu, C.-H. Lu, and J. O. Roads, 2007: A comparison of the Noah and OSU land surface models in the ECPC Seasonal Forecast Model. *J. Hydrometeor.,* **8,** 1031–1048.

Desborough, C. E., A. J. Pitman, and B. J. McAvaney, 2001: Surface energy balance complexity in GCM land surface models. Part II: Coupled simulations. *Climate Dyn.,* **17,** 615–626.

Dirmeyer, P. A., and F. J. Zeng, 1999: An update to the distribution and treatment of vegetation and soil properties in SSiB. Center for Ocean–Land–Atmosphere Studies Tech. Rep. 78, 25 pp.

——, X. Gao, M. Zhao, Z. Guo, T. Oki, and N. Hanasaki, 2006: GSWP-2: Multimodel analysis and implications for our perception of the land surface. *Bull. Amer. Meteor. Soc.,* **87,** 1381–1397.

Ek, M. B., K. E. Mitchell, Y. Lin, E. Rogers, P. Grunmann, V. Koren, G. Gayno, and J. D. Tarpley, 2003: Implementation of Noah land surface model advances in the National Centers for Environmental Prediction operational mesoscale Eta model. *J. Geophys. Res.,* **108,** 8851, doi:10.1029/2002JD003296.

Gates, W., 1992: AMIP: The Atmospheric Model Intercomparison Project. *Bull. Amer. Meteor. Soc.,* **73,** 1962–1970.

Gedney, N., P. M. Cox, H. Douville, J. Polcher, and P. J. Valdes, 2000: Characterizing GCM land surface schemes to understand their responses to climate change. *J. Climate,* **13,** 3066–3079.

Guo, Z., and P. A. Dirmeyer, 2006: Evaluation of the Second Global Soil Wetness Project soil moisture simulations: 1. Intermodel comparison. *J. Geophys. Res.,* **111,** D22S02, doi:10.1029/2006JD007233.

——, ——, Z.-Z. Hu, X. Gao, and M. Zhao, 2006a: Evaluation of the Second Global Soil Wetness Project soil moisture simulations: 2. Sensitivity to external meteorological forcing. *J. Geophys. Res.,* **111,** D22S03, doi:10.1029/2006JD007845.

——, and Coauthors, 2006b: GLACE: The Global Land–Atmosphere Coupling Experiment. Part II: Analysis. *J. Hydrometeor.,* **7,** 611–625.

Henderson-Sellers, A., A. J. Pitman, P. K. Love, P. Irannejad, and T. Chen, 1995: The Project for Intercomparison of Land Surface Parameterization Schemes (PILPS): Phases 2 and 3. *Bull. Amer. Meteor. Soc.,* **76,** 489–503.

——, and Coauthors, 1996: The Project for Intercomparison of Land-surface Parameterization Schemes (PILPS): 1992 to 1995. *Climate Dyn.,* **12,** 849–859.

——, P. Irannejad, K. McGuffie, and A. J. Pitman, 2003: Predicting land-surface climates-better skill or moving targets? *Geophys. Res. Lett.,* **30,** 1777, doi:10.1029/2003GL017387.

Hong, S. Y., and H. L. Pan, 1996: Nonlocal boundary layer vertical diffusion in a medium range forecast model. *Mon. Wea. Rev.,* **124,** 2322–2339.

Hu, Q., and S. Feng, 2004: Why has the land memory changed? *J. Climate,* **17,** 3236–3243.

Irannejad, P., A. Henderson-Sellers, and S. Sharmeen, 2003: Importance of land-surface parameterization for latent heat simulation in global atmospheric models. *Geophys. Res. Lett.,* **30,** 1904, doi:10.1029/2003GL018044.

Karl, T., and Coauthors, 1993: A new perspective on recent global warming: Asymmetric trends of daily maximum and minimum temperature. *Bull. Amer. Meteor. Soc.,* **74,** 1007–1023.

Kato, H., M. Rodell, F. Beyrich, H. Cleugh, E. van Gorsel, and H. Liu, 2007: Sensitivity of land surface simulations to model physics, land characteristics, and forcings, at four CEOP sites. *J. Meteor. Soc. Japan,* **85A,** 187–204.

Kiehl, J. T., J. J. Hack, G. B. Bonan, B. A. Boville, D. L. Williamson, and P. J. Rasch, 1998: The National Center for Atmospheric Research Community Climate Model: CCM3. *J. Climate,* **11,** 1131–1149.

Kinter, J. L., and Coauthors, 1997: The COLA atmosphere-biosphere general circulation model. Vol. 1: Formulation. Center for Ocean–Land–Atmosphere Studies Tech. Rep. 51, 46 pp.

Kirtman, B. P., and J. Shukla, 2002: Interactive coupled ensemble: A new coupling strategy for CGCMs. *Geophys. Res. Lett.,* **29,** 1367, doi:10.1029/2002GL014834.

Koren, V., J. Schaake, K. Mitchell, Q.-Y. Duan, F. Chen, and J. M. Baker, 1999: A parameterization of snowpack and frozen ground intended for NCEP weather and climate models. *J. Geophys. Res.,* **104** (D16), 19 569–19 585.

Koster, R. D., and M. J. Suarez, 1992: Modeling the land surface boundary in climate models as a composite of independent vegetation stands. *J. Geophys. Res.,* **97,** 2697–2716.

——, and ——, 1996: The influence of land surface moisture retention on precipitation statistics. *J. Climate,* **9,** 2551–2567.

——, and ——, 2001: Soil moisture memory in climate models. *J. Hydrometeor.,* **2,** 558–570.

——, ——, R. W. Higgins, and H. M. Van den Dool, 2003: Observational evidence that soil moisture variations affect precipitation. *Geophys. Res. Lett.,* **30,** 1241, doi:10.1029/2002GL016571.

——, and Coauthors, 2006: GLACE: The Global Land–Atmosphere Coupling Experiment. Part I: Overview. *J. Hydrometeor.,* **7,** 590–610.

Leplastrier, M., A. J. Pitman, H. Gupta, and Y. Xia, 2002: Exploring the relationship between complexity and performance in a land surface model using the multicriteria method. *J. Geophys. Res.,* **107,** 4443, doi:10.1029/2001JD000931.

Liang, X., and Coauthors, 1998: The Project for Intercomparison of Land-surface Parameterization Schemes (PILPS) phase 2(c) Red-Arkansas River basin experiment: 2. Spatial and temporal analysis of energy fluxes. *Global Planet. Change,* **19,** 137–159.

Misra, V., and Coauthors, 2007: Validating and understanding ENSO simulation in two coupled climate models. *Tellus,* **59A,** 292–308.

Moorthi, S., and M. J. Suarez, 1992: Relaxed Arakawa–Schubert. A parameterization of moist convection for general circulation models. *Mon. Wea. Rev.,* **120,** 978–1002.

Niu, G.-Y., Z.-L. Yang, R. E. Dickinson, and L. E. Gulden, 2005: A simple TOPMODEL-based runoff parameterization (SIMTOP)

for use in global climate models. *J. Geophys. Res.,* **110,** D21106, doi:10.1029/2005JD006111.

——, ——, ——, ——, and H. Su, 2007: Development of a simple groundwater model for use in climate models and evaluation with Gravity Recovery and Climate Experiment data. *J. Geophys. Res.,* **112,** D07103, doi:10.1029/2006JD007522.

Oleson, K. W., and Coauthors, 2004: Technical description of the Community Land Model (CLM). NCAR Tech. Note NCAR/TN-461+STR, 173 pp.

——, and Coauthors, 2008: Improvements to the Community Land Model and their impact on the hydrological cycle. *J. Geophys. Res.,* **113,** G01021, doi:10.1029/2007JG000563.

Pan, H.-L., and L. Mahrt, 1987: Interaction between soil hydrology and boundary layer developments. *Bound.-Layer Meteor.,* **38,** 185–202.

Phillips, T., 1994: A summary documentation of the AMIP models. PCMDI Rep. 18, Lawrence Livermore National Laboratory UCRL-ID-116348, 343 pp.

Pitman, A. J., and A. Henderson-Sellers, 1998: Recent progress and results from the project for the intercomparison of land surface parameterization schemes. *J. Hydrol.,* **212–213,** 128–135.

——, and Coauthors, 1999: Key results and implications from phase 1(c) of the Project for Intercomparison of Land-Surface Parameterization Schemes. *Climate Dyn.,* **15,** 673–684.

——, B. J. McAvaney, N. Bagnoud, and B. Cheminat, 2004: Are inter-model differences in AMIP-II near surface air temperature means and extremes explained by land surface energy balance complexity? *Geophys. Res. Lett.,* **31,** L05205, doi:10.1029/2003GL019233.

——, and Coauthors, 2009: Uncertainties in climate responses to past land cover change: First results from the LUCID intercomparison study. *Geophys. Res. Lett.,* **36,** L14814, doi:10.1029/2009GL039076.

Polcher, J., and Coauthors, 1998: Importance of land-surface processes for the uncertainties of climate change: A European Project. *GEWEX News,* No. 8, International GEWEX Project Office, Silver Spring, MD, 11–13.

Qu, W. Q., and A. Henderson-Sellers, 1998: Comparing the scatter in PILPS off-line experiments with that in AMIP I coupled experiments. *Global Planet. Change,* **19,** 209–223.

Reynolds, R. W., N. A. Rayner, T. M. Smith, D. C. Stokes, and W. Wang, 2002: An improved in situ and satellite SST analysis for climate. *J. Climate,* **15,** 1609–1625.

Rudolf, B., H. Hauschild, W. Reuth, and U. Schneider, 1994: Terrestrial precipitation analysis: Operational method and required density of point measurements. *Global Precipitation and Climate Change,* M. Desbois, F. Desalmond, Eds., NATO ASI Series I, Vol. 26, Springer-Verlag, 173–186.

Sellers, P. J., and Coauthors, 1997: Modelling the exchanges of energy, water and carbon between continents and the atmosphere. *Science,* **275,** 502–509.

Stieglitz, M., A. Ducharne, R. Koster, and M. Suarez, 2001: The impact of detailed snow physics on the simulation of snow cover and subsurface thermodynamics at continental scales. *J. Hydrometeor.,* **2,** 228–242.

Timbal, B., and A. Henderson-Sellers, 1998: Intercomparisons of land-surface parameterizations coupled to a limited area forecast model. *Global Planet. Change,* **19,** 247–260.

Uppala, S. M., and Coauthors, 2005: The ERA-40 Re-Analysis. *Quart. J. Roy. Meteor. Soc.,* **131,** 2961–3012, doi:10.1256/qj.04.176.

Wei, J., R. E. Dickinson, and N. Zeng, 2006: Climate variability in a simple model of warm climate land-atmosphere interaction. *J. Geophys. Res.,* **111,** G03009, doi:10.1029/2005JG000096.

——, ——, and H. Chen, 2008a: A negative soil moisture–precipitation relationship and its causes. *J. Hydrometeor.,* **9,** 1364–1376.

——, P. A. Dirmeyer, and Z. Guo, 2008b: Sensitivities of soil wetness simulation to uncertainties in precipitation and radiation. *Geophys. Res. Lett.,* **35,** L15703, doi:10.1029/2008GL034494.

——, ——, and ——, 2009: Sensitivities of simulated soil wetness and surface fluxes to uncertainties in atmospheric forcing. Center for Ocean–Land–Atmosphere Studies Tech. Rep. 278, 25 pp. [Available online at ftp://grads.iges.org/pub/ctr/CTR278_ms.pdf.]

——, ——, and ——, 2010: How much do different land models matter for climate simulation? Part II: A decomposed view of the land–atmosphere coupling strength. *J. Climate,* **23,** 3135–3145.

Wilks, D. S., 2006: *Statistical Methods in the Atmospheric Sciences.* 2nd ed. Academic Press, 141 pp.

Xie, P., J. E. Janowiak, P. A. Arkin, R. Adler, A. Gruber, R. Ferraro, G. J. Huffman, and S. Curtis, 2003: GPCP pentad precipitation analyses: An experimental dataset based on gauge observations and satellite estimates. *J. Climate,* **16,** 2197–2214.

Xue, Y., P. J. Sellers, J. L. Kinter, and J. Shukla, 1991: A simplified biosphere model for global climate studies. *J. Climate,* **4,** 345–364.

——, H.-M. H. Juang, W.-P. Li, S. Prince, R. DeFries, Y. Jiao, and R. Vasic, 2004: Role of land surface processes in monsoon development: East Asia and West Africa. *J. Geophys. Res.,* **109,** D03105, doi:10.1029/2003JD003556.

——, F. de Sales, W.-P. Li, C. R. Mechoso, C. A. Nobre, and H.-M. Juang, 2006: Role of land surface processes in South American monsoon development. *J. Climate,* **19,** 741–762.

Yang, F., A. Kumar, W. Wang, H. M. H. Juang, and M. Kanamitsu, 2001: Snow–albedo feedback and seasonal climate variability over North America. *J. Climate,* **14,** 4245–4248.

Zeng, N., and J. D. Neelin, 1999: A land–atmosphere interaction theory for the tropical deforestation problem. *J. Climate,* **12,** 857–872.

Zhou, L., R. E. Dickinson, Y. Tian, R. S. Vose, and Y. Dai, 2007: Impact of vegetation removal and soil aridation on diurnal temperature range in a semiarid region: Application to the Sahel. *Proc. Natl. Acad. Sci. USA,* **104,** 17 937–17 942.

——, ——, P. Dirmeyer, H. Chen, Y. Dai, and Y. Tian, 2008: Asymmetric response of maximum and minimum temperatures to soil emissivity change over the Northern African Sahel in a GCM. *Geophys. Res. Lett.,* **35,** L05402, doi:10.1029/2007GL032953.